In situ observations of the effect of a solar wind compression on Saturn's magnetotail

Caitriona M. Jackman, Christopher S. Arridge, James A. Slavin, Steve E. Milan, Laurent Lamy, Michele K. Dougherty, A. J. Coates

In situ observations of the effect of a solar wind compression on Saturn's magnetotail

C. M. Jackman,[1] C. S. Arridge,[2,3] J. A. Slavin,[4] S. E. Milan,[5] L. Lamy,[1] M. K. Dougherty,[1] and A. J. Coates[2,3]

Received 27 January 2010; revised 13 May 2010; accepted 25 May 2010; published 22 October 2010.

[1] In this paper we explore the dynamic response of Saturn's magnetotail to an episode of solar wind compression that took place while Cassini was sampling Saturn's nightside equatorial magnetosphere in 2006. Following an initial increase in solar wind dynamic pressure the magnetosphere was compressed, but over several subsequent days the flaring of the tail increased as open flux built up in the tail lobes. Several days later the current sheet was displaced southward from its previously hinged position, and magnetic signatures consistent with the passage of a plasmoid were observed. Concurrently, Saturn's kilometric radio emissions were enhanced and the spectrum displayed a continuous extension to lower frequency, corresponding to radio sources detected at higher altitudes. We suggest that all of the above features are a common consequence of the impact of a solar wind compression on Saturn's magnetosphere.

Citation: Jackman, C. M., C. S. Arridge, J. A. Slavin, S. E. Milan, L. Lamy, M. K. Dougherty, and A. J. Coates (2010), In situ observations of the effect of a solar wind compression on Saturn's magnetotail, *J. Geophys. Res.*, *115*, A10240, doi:10.1029/2010JA015312.

1. Introduction

1.1. Earth

[2] The Earth's magnetosphere has a long magnetic tail with a current sheet at its center separating northern and southern lobes of oppositely directed magnetic field lines. The magnetotail radius increases with distance from the planet until ~120 R_E (1 R_E = 6378 km) downtail before the flaring ceases [*Slavin et al.*, 1985]. Beyond this point the field strength in the magnetotail lobes is approximately constant and is balanced by the solar wind field and thermal pressure.

[3] The magnetotail lobes house the open flux within the magnetosphere. Changes in the flux content arise in response to competition between the rate of reconnection at the dayside magnetopause where flux is opened and the rate of reconnection in the magnetotail where flux is closed. The open flux content of the terrestrial lobes is estimated to range from ~0.2 to 1 GWb [*Milan et al.*, 2007]. Factors such as the static and dynamic pressures of the solar wind and the interplanetary magnetic field (IMF) B_z component dictate the reconnection rates and in turn the open flux level. It may be influenced by the recent history of the solar wind properties as well as the simultaneous values. "Sudden impulses" where the open flux (and hence the lobe field strength) increases on time scales of a few minutes have been reported by several authors [e.g., *Collier et al.*, 1998; *Huttunen et al.*, 2005]. Meanwhile, short, intense bursts of flux closure in the magnetotail have been found to be directly driven by compression of the magnetosphere by interplanetary shocks which represent strong and rapid variations in solar wind pressure [*Milan et al.*, 2004; *Hubert et al.*, 2006]. The effect of such rapid solar wind changes has also been explored by *Boudouridis et al.* [2003] who found significant changes in the size, location, and intensity of the auroral oval.

[4] In addition, internal dynamics associated with magnetospheric substorms that operate on time scales of order tens of minutes may modulate the amount of open flux in the magnetosphere, and hence the lobe field strength. During the "growth phase" of terrestrial substorms, energy from the solar wind can be transferred to the magnetotail through the interaction of the interplanetary magnetic field with the planetary field across the magnetopause [e.g., *McPherron*, 1970]. The magnetotail then flares at a greater angle to the solar wind flow, and this leads to the enhancement in tail lobe field strength and consequently the magnetic pressure [e.g., *Coroniti and Kennel*, 1972; *Russell and McPherron*, 1973]. The flaring angle is thus dictated by the amount of open flux contained within the magnetotail. Following substorm onset the field may exhibit a local spike due to the compression of the lobes by tailward-moving plasmoids. Such field deflections are known as traveling compression regions (TCRs) and occur as bubbles of closed magnetic flux known as plasmoids squeeze down the tail following reconnection [*Slavin et al.*,

[1]Blackett Laboratory, Imperial College London, London, UK.
[2]Mullard Space Science Laboratory, Department of Space and Climate Physics, University College London, Dorking, UK.
[3]The Centre for Planetary Sciences at UCL/Birkbeck, London, UK.
[4]Heliophysics Science Division, NASA Goddard Space Flight Center, Greenbelt, Maryland, USA.
[5]Radio and Space Plasma Physics Group, University of Leicester, Leicester, UK.

0148-0227/10/2010JA015312

1984]. After substorm onset the field strength will typically decrease, corresponding to closure of flux and a resultant deflation of the tail [e.g., *Milan et al.*, 2004, 2008].

1.2. Saturn

[5] A number of studies have explored the influence of the solar wind on magnetospheric dynamics at Saturn. Using data from the Saturn Orbit Insertion (SOI) pass, *Bunce et al.* [2005] showed evidence of compression-induced magnetotail collapse. Following a strong solar wind compression of the magnetosphere on the outbound pass of SOI, the auroral Saturn kilometric radiation (SKR) intensified, the magnetic field became depressed and changed orientation, and the electron and ion observations showed that the spacecraft was surrounded by hot, tenuous plasma. Thus, they interpreted the interval as representing a large magnetotail reconnection event accompanied by hot plasma injection.

[6] Several other authors have noted that shock compressions in the solar wind can have direct effects on both the SKR emissions and the auroral output [e.g., *Desch and Rucker*, 1983; *Clarke et al.*, 2005; *Crary et al.*, 2005; *Kurth et al.*, 2005]. The brightenings and subsequent poleward expansion of the UV auroral emissions observed during the January 2004 Cassini-HST (Hubble Space Telescope) campaign were interpreted by *Cowley et al.* [2005] as related to compression-induced reconnection. They suggested that following a strong solar wind compression, magnetotail reconnection closes a significant fraction of the open flux in the tail lobes. These newly closed flux tubes then subcorotate in the outer magnetosphere and give rise to the spiral structures observed in the auroral images. Using the auroral images from the January 2004 Cassini-HST campaign, *Badman et al.* [2005] took the poleward edge of each of the images as a proxy for the open-closed field line boundary and estimated the amount of open flux within this region. They found that the open flux content of the southern polar region ranged from ~15 to 50 GWb over the interval studied, which they interpreted as due to a significant interaction between Saturn's magnetosphere and the solar wind, which was highly structured by corotating interaction region compressions and rarefactions during the declining phase of the solar cycle.

[7] Since SOI, Cassini has performed many orbits inside Saturn's magnetosphere, and in 2006, the spacecraft entered a phase of equatorial deep-tail orbits, ideal conditions for the in situ observation of the effects of magnetotail reconnection. To date, nine examples in total have been recorded in the literature, and their specific characteristics are discussed in detail by *Jackman et al.* [2007, 2008a, 2009a] and *Hill et al.* [2008]. *Milan et al.* [2005] developed a time-dependent model of the kronian magnetotail that invokes twisted tail lobes (originally postulated by *Isbell et al.* [1984]), with older field lines at the core surrounded by bundles of newer field lines disconnected by tail reconnection and propagating down-tail at the solar wind speed. The tail is found to inflate during periods of solar wind-magnetosphere coupling via dayside reconnection, and this inflation stretches downtail at the solar wind speed. The length of the inflated tail is governed by the time since the last episode of tail reconnection. Thus, flux transport in Saturn's magnetotail can best be described as a "last-in-first-out" system, in contrast to the case of the Earth which is "first-in-first-out" in terms of flux removal [*Milan*, 2004; *Milan et al.*, 2004].

[8] One additional effect that the solar wind induces on Saturn's magnetosphere is the observed hinging of the magnetotail. This was reported by *Arridge et al.* [2008] who noted from spacecraft observations during Southern Hemisphere summer that Saturn's current sheet is displaced above the planet's rotational equator and forms a bowl shape. The implication of this for spacecraft orbiting in the equatorial plane, as we will see later, is that they can be situated well below the nominal position of the current sheet.

[9] In this paper we show a case study example from Saturn's magnetotail that illustrates the response of Saturn's magnetotail to solar wind compression. We explore changes in magnetotail flaring and flux content and examine the response of auroral radio emissions to sudden solar wind changes. We also look at episodes of magnetic reconnection and current sheet motion with a view to deciphering the time scales and precise conditions required for the tail to respond dynamically to conditions external to the magnetosphere.

2. Observations

[10] For this paper we use data from three instruments on Cassini. First, we use data from the magnetometer [*Dougherty et al.*, 2004] at 1 s resolution and with an uncertainty of <1%. Second, we use data from the electron spectrometer (ELS), part of the Cassini Plasma Spectrometer (CAPS) suite of instruments [*Young et al.*, 2004], with electron density moments as derived and used in the survey of *Arridge et al.* [2009]. Finally, we employ data from the radio and plasma wave science (RPWS) instrument that provides information on Saturn's radio emissions [*Gurnett et al.*, 2004]. SKR is an auroral emission, observed remotely and continuously, and here we use the data processed as outlined in the study by *Lamy et al.* [2008].

[11] In the absence of an upstream monitor we also use propagated values for solar wind velocity and dynamic pressure, as derived from the mSWiM (Michigan Solar Wind Model) model [*Zieger and Hansen*, 2008]. This model uses a one-dimensional numerical MHD code to propagate hourly averaged solar wind data from 1 AU outward. For the purposes of propagation modeling, the solar wind in 2006 had the highest recurrence index of any year since 1974, and thus, the propagations during this period may be regarded as the most accurate of the Cassini era. However, there is a finite error on the prediction of solar wind shock arrival times, and this error is related to the length in time from opposition (when the Earth and the spacecraft are located around the same helioecliptic longitude). Apparent opposition occurs some time later, when the solar wind as seen at Earth arrives at the spacecraft (estimated in this model by taking a constant solar wind velocity of 500 km/s). Apparent opposition (when the propagation is most accurate) occurred on day 56 of 2006, and thus, the interval that we study here is ~70 days from this point. As such, the error on shock arrival is likely to be of order ±22 h (B. Zieger, personal communication, 2010). We have attempted to account for this error by smoothing the solar wind dynamic pressure and velocity profiles according to this shock arrival time error. Thus, at each point, rather than using the pressure and velocity as derived directly from the model, we take an

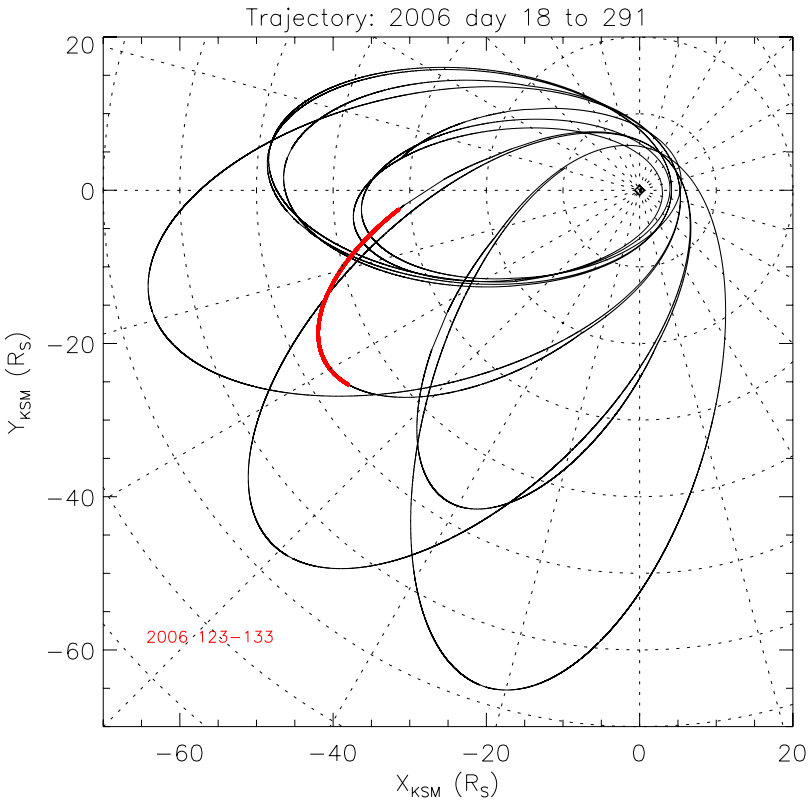

Figure 1. Equatorial view of the trajectory of Cassini during the period 2006 days 18–291. Dashed lines mark hours of local time (LT) and circles of constant radial distance, in 10 R_S steps. The case study interval is highlighted in red.

average of all points 22 h either side of each measurement. Thus, we obtain a "smoothed" profile where the shocks are less sharp but where the general cadence of the propagated data is preserved.

[12] The Cassini spacecraft has been in orbit around Saturn since July 2004, but the deep magnetotail was first explored in detail in 2006 when the spacecraft executed a series of orbits that reached downtail distances of ~68 R_S, primarily on the dawn side. *Jackman et al.* [2009b] looked in detail at the typical properties of the lobes and current sheet at Saturn during the interval from 2006 days 18–291. They identified lobe regions by quiet field and low-density plasma, whereas current sheet regions were centered near reversals in the radial magnetic field component as well as local density maxima. The precise criteria are defined in their work, and we use their result for the falloff of lobe field strength with radial distance downtail: $B_{\rm lobe}$ (nT) = 200 × $R^{-1.2}$. Figure 1 shows the trajectory of Cassini in the equatorial plane during this period of 2006, with the case study interval highlighted in red.

3. Example: 2006 Days 123-133

[13] In Figure 2 we show radio, plasma, and magnetometer data from the interval 2006 days 123–133, during which Cassini was sampling the kronian magnetotail at radial distances between ~33 and 48.5 R_S. The magnetic field data is shown in kronocentric spherical co-ordinates, where the radial component (B_r) is positive outward from Saturn, the theta component (B_θ) is positive southward, and the azimuthal component (B_φ) is positive in the direction of corotation (in a prograde direction). This system is ideal for observing dynamics in the magnetotail, where strong changes in the north-south component can be indicative of reconnection

Figure 2. Radio, plasma, and magnetometer data for the interval covering 2006 days 123–133. (a) A frequency-time spectrogram of the radio emission with low-frequency extensions (LFEs) marked by solid horizontal bars on top. (b) An energy-time electron spectrogram from CAPS/ELS (Cassini Plasma Science-Electron Spectrometer). (c) Propagated solar wind radial velocity from the mSWiM model [*Zieger and Hansen*, 2008] as dashed line and corrected (smoothed) velocity as solid line. (d) Propagated solar wind dynamic (dashed) and corrected (solid) pressure and magnetic pressure inside magnetosphere in red. (e) α, the flaring angle; (f) components of the magnetic field in kronocentric spherical, KRTP, co-ordinates; (g) total magnetic field strength with lobe and current sheet intervals overplotted in blue and red, respectively. The dotted line represents the average lobe field strength at each radial distance from $B_{\rm lobe}$ = 200 × $R^{-1.2}$, with dashed lines showing one standard deviation either side. Day number, radial range, magnetic latitude, and Saturn local time (LT) are displayed at the bottom of the figure.

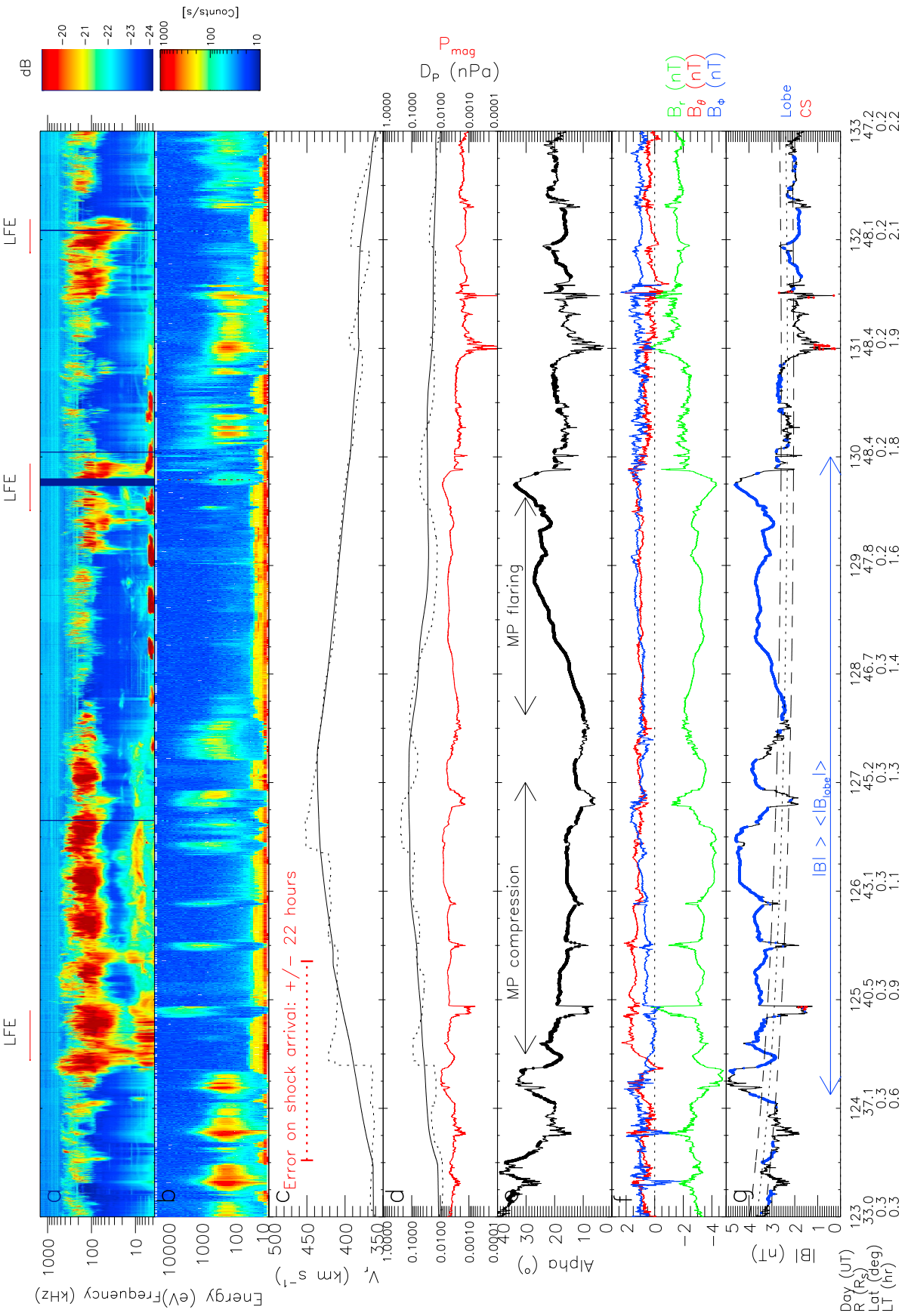
a
b
c
d
e
f
g
LFE
LFE
LFE
dB
[Counts/s]
Energy (eV)/Frequency (kHz)
Error on shock arrival: +/- 22 hours
V_r (km s^{-1})
P_{mag}
D_P (nPa)
MP compression
MP flaring
Alpha (°)
B_r (nT)
B_θ (nT)
B_ϕ (nT)
Lobe
CS
|B| > <$|B_{lobe}|$>
|B| (nT)
Day (UT)
R (R_S)
Lat (deg)
LT (hr)

Figure 2

processes [e.g., *Jackman et al.*, 2009c]. Figures 2c–2d show the propagated solar wind velocity and dynamic pressure, as derived from the mSWiM model [*Zieger and Hansen*, 2008]. The error on shock arrival of ±22 h is marked on the plot as a horizontal dashed bar. This must be taken into consideration when comparing with the timing of features in the in situ magnetospheric data. The solar wind velocity and dynamic pressure values as taken directly from the propagation model are shown by dotted lines, and the smoothed values, corrected for shock arrival time (as described in section 2), are shown by the solid lines.

[14] We present a spectrogram of the radio emissions as measured by the RPWS instrument in Figure 2a. SKR peaks in the ~100–400 kHz range, where sudden enhancements can be used to good effect as a proxy for solar wind compressions [e.g., *Desch and Rucker*, 1983; *Bunce et al.*, 2005; *Kurth et al.*, 2005; *Jackman et al.*, 2005]. In addition, extensions of the spectrum toward lower frequencies (as low as a few kHz) have been observed to correspond to reconnection events in Saturn's magnetotail [*Jackman et al.*, 2009a]. This is similar to what has been reported at Earth, where substorm activity generates intense auroral kilometric radiation [e.g., *Gurnett*, 1974]. The frequency of radio emission is inversely proportional to the altitude of the radio source along the field line, due to the fact that the emission is generated at or close to the local electron cyclotron frequency. *Morioka et al.* [2008] proposed that substorms at Earth can also be associated with lower frequency radio emission, which corresponds to radio sources at higher altitudes. For the case of Saturn, kilometric low-frequency extensions (LFEs) are characterized by intense radio emission stretching from the main 100–400 kHz band down to lower frequencies. It is important to make the distinction between those LFEs and narrowband emissions appearing below ~40 kHz (simultaneously to LFEs on Figure 2), which, unlike the SKR, are not thought to be generated by the cyclotron maser instability. There are two categories of narrowband emission: intense, weakly polarized, low-frequency (<10 kHz) periodic bursts that are suggested to be linked with plasma evacuation from the disk [*Louarn et al.*, 2007], and a more diffuse, strongly circularly polarized component between 10–40 kHz [e.g., *Gurnett et al.*, 1981; *Lamy et al.*, 2008; *Ye et al.*, 2009]. For the purposes of this work we will focus primarily on the LFEs as opposed to the narrowband components of the radio spectrum.

[15] First, we will focus on the immediate effects of a solar wind compression on Saturn's magnetosphere. As mentioned in section 1.2, SKR emissions can be used as a good indicator of solar wind activity. As seen in Figure 2, from ~08:00 on day 124 we observe a strong burst of intense radio emission. This burst was followed by a continuous extension of the spectrum to frequencies below 10 kHz. Distinct from this, we note the appearance of quasi-periodic lower-frequency radio emissions (around ~3 kHz) beginning at the same time and then drifting in frequency, as well as more diffuse low-frequency emissions that also appear to drift somewhat toward higher frequencies through days 127–128. Figure 3a is a zoom-in of days 123–125, the first 2 days of the interval shown in Figure 2. This zoom-in enables the finer details of the timing of particular features to be seen more clearly. We note that from ~03:00 on day 124 (time *i*), the field strength in the tail rose above the typical lobe field magnitude (as denoted by the dotted line in the bottom frame). This initial increase is closely correlated in time with two other effects: the burst of radio emission mentioned above and the passage of an interplanetary shock. Close to the time of the SKR enhancement, there was a clear step increase in solar wind velocity and dynamic pressure, beginning at ~10:00 on day 124 (time *ii*). These features combined strongly suggest that the magnetosphere underwent a significant solar wind compression during this time. It seems likely that the precise timing of the solar wind dynamic pressure increase may have been several hours in advance of what is seen here, in order that the shock compression impact may have driven the tail field increase, and this is well within the error margin of the propagations. For example, a compression traveling from a magnetopause at 25 R_S to a downtail distance of 30 R_S at a solar wind speed of 300 km/s would take just over 3 h. We also note that the B_θ component underwent a 1 nT reduction centered on ~09:00 of day 124 and even turned briefly northward, coincident with a small local increase in the field strength, on top of the larger trend. We suggest from the geometry of the observation that Cassini was situated tailward of a reconnection site and observing the passage of a small TCR, the result of a brief interval of tail reconnection induced by the shock compression of the magnetosphere. The plasmoid that caused the TCR signature was most likely released several minutes earlier from a position planetward of 38 R_S.

[16] Solar wind compression will have an effect on the shape of the magnetopause boundary. The degree of flaring of this boundary can provide indirect information about the amount of open flux contained within the magnetotail lobes. Studies at Earth assumed that the total pressure in the lobes of the magnetotail is balanced by the total pressure of the solar wind incident on the magnetopause (e.g., *Petrinec and Russell* [1996])

$$\frac{\left(B_T^2\right)_{\mathrm{LOBE}}}{2\mu_0} = K\rho v_{\mathrm{SW}}^2 \sin^2\alpha + \frac{\left(B_T^2\right)_{\mathrm{SW}}}{2\mu_0} + \left[nk(T_i + T_e)\right]_{\mathrm{SW}}, \quad (1)$$

where α (the flaring angle) denotes the angle between the solar wind flow direction and the tangent to the magnetopause. α is 90° at the nose of the magnetopause, reducing to 0° in the deep tail when the flaring asymptotes. The constant K is set to 0.881 that is valid in high Mach number regimes [*Spreiter and Alksne*, 1970], and thus has been found to be appropriate for use at Saturn [*Achilleos et al.*, 2006; *Arridge et al.*, 2006]. The distant magnetotail is found to asymptote at a downtail distance of ~220 R_S at Saturn [*Arridge et al.*, 2006]. Thus, our observations for this study, which all take place inside of 49 R_S, place Cassini well within the flared

Figure 3. (a) Zoom-in of radio, plasma, and magnetometer data for the interval 2006 days 123–125 in same format as Figure 2. Vertical solid lines represent (*i*) B lobe increase and (*ii*) SKR burst with jump in solar wind velocity and dynamic pressure. (b) Zoom-in of radio, plasma, and magnetometer data for the interval 2006 days 129–132 in same format as Figure 2. (*i*) and (*ii*) are two current sheet encounters.

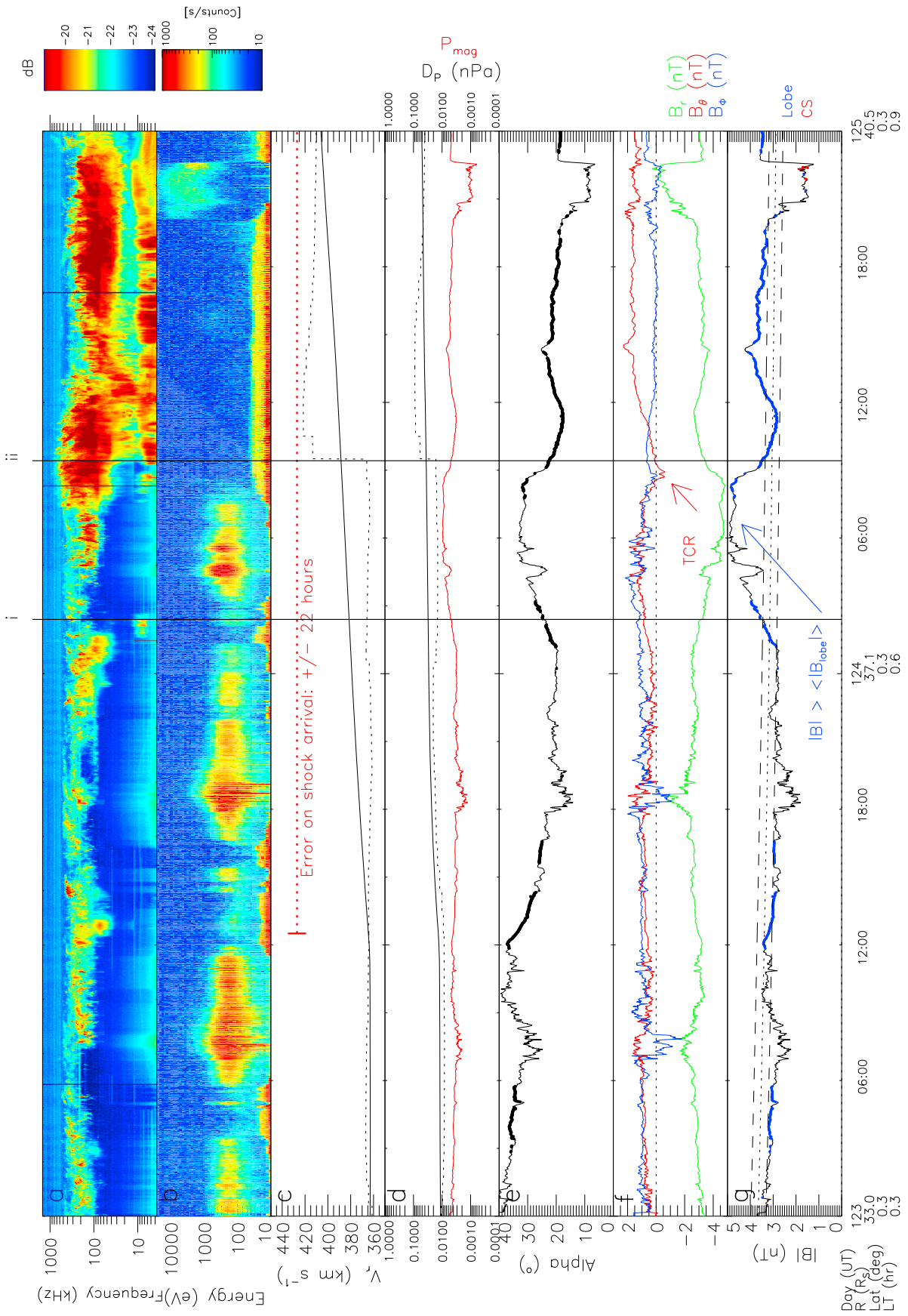
dB
[counts/s]
P_mag
D_P (nPa)
Error on shock arrival: +/− 22 hours
B_r (nT)
B_θ (nT)
B_φ (nT)
Lobe
CS
TCR
|B| > <|B_lobe|>
Energy (eV)/Frequency (kHz)
V_r (km s^-1)
Alpha (°)
|B| (nT)
Day (UT)
R (R_S)
Lat (deg)
LT (hr)

Figure 3

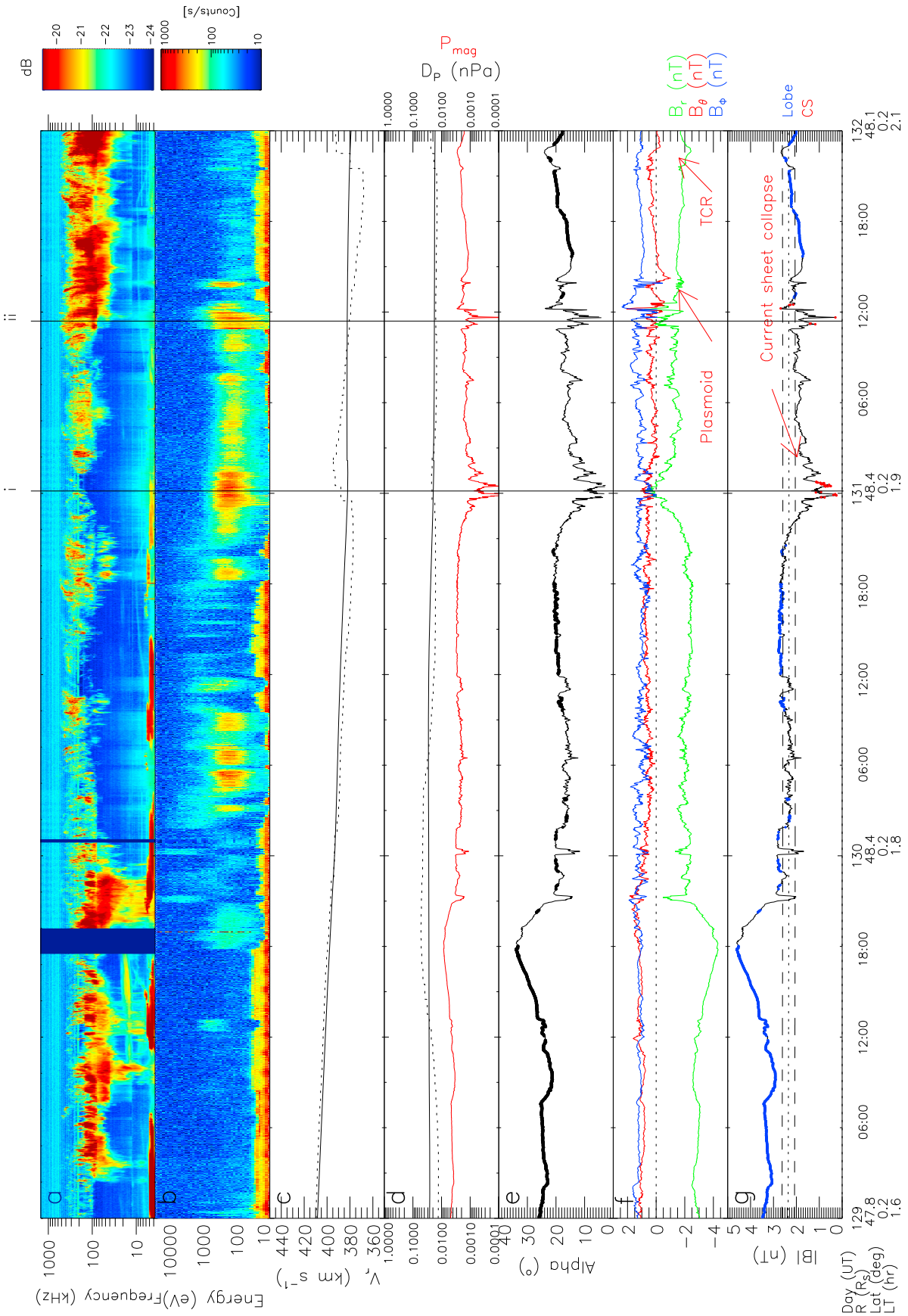

Figure 3. (continued)

regime. As such, we can assume that the contribution of the thermal pressure is negligible compared to the other terms on the right-hand side of equation (1). We thus ignore the last term and solve for α, which is then plotted in the fifth panel (e) of Figures 2, 3a, and 3b. We use the instantaneous magnetic pressure in the lobes, combined with the corrected (smoothed) solar wind dynamic and magnetic pressures for this calculation.

[17] We note that with the sharp increase in lobe field strength at the start of day 124, the flaring angle increases (see equation (1)) briefly. It then decreases some hours later and remains low for several days before slowly growing from the middle of day 127 onward. The overall profile of total field strength shows an elevation above typical lobe conditions for ~7 days after the initial solar wind compression on day 124. For most of this time the conditions were "lobe-like" with quiet fields and a negative radial component indicating that Cassini was situated below the nominal current sheet location. As detailed in the introduction, during Southern Hemisphere summer, Saturn's current sheet is expected to be hinged upward out of the rotational equator due to the influence of the solar wind, and thus, equatorial orbits can largely occur beneath the nominal current sheet location in the southern lobe [*Arridge et al.*, 2008]. On day 124 at ~22:00 there was a notable exception to the quiet, elevated field strengths. Despite the spacecraft maintaining an approximately constant latitude, the B_r component rapidly shifted by ~3 nT and the spacecraft encountered the center of the current sheet ($B_r = 0$). The ELS spectrogram in the second panel in Figure 2 displayed some unusually high energy electrons at this time, and we note that the electron temperature typically varies by no more than a factor of 2 between the central plasma sheet and the lobes [*Arridge et al.*, 2009], suggesting that this energization is the result of magnetotail dynamics.

[18] With the exception of this brief current sheet encounter, the following days 125–130 were characterized by extended periods of largely lobe-like behavior and elevated solar wind dynamic pressure. However, as can be seen more clearly in the zoomed-in plot in Figure 3b (which covers days 129–132), the character of the field and plasma changed quite dramatically from the end of day 129. The lobe field strength sharply dropped at this time, and the SKR was enhanced along with the appearance of low-frequency emissions. At this time we see no clear evidence of a magnetotail reconnection signature, but the field became significantly noisier, and we note the appearance of more energized plasma indicative of the spacecraft's presence in the disturbed outer plasma sheet [*Arridge et al.*, 2009].

[19] This continued until ~23:30 on day 130 when the field strength dropped once more and Cassini encountered the center of the current sheet twice: first at the very start of day 131 (*i*) and then again at ~12:00 on day 131 (*ii*). Both encounters are associated with a quiet time plasma sheet with local electron density maxima (not shown) [*Arridge et al.*, 2009]. Shortly after the second encounter, at ~14:00 on day 131, the B_θ component exhibited a northward turning and slow recovery, with a total field deflection of magnitude ~1.8 nT (marked with an arrow on Figure 3b). Another smaller northward turning of the field was observed at the very end of day 131, from ~22:30 when Cassini had moved further away from the current sheet and was in the lobe. We suggest that these signatures indicate the passage of at least one, if not multiple plasmoids across or near the spacecraft following a magnetotail reconnection event. These signatures were accompanied by enhanced SKR emission with some extension of the spectrum to lower frequency.

[20] Finally, from the start of day 132 onward (Figure 2) the spacecraft dipped in and out of lobe-like regions and the tail returned to what we would expect of typical "quiet" conditions at this radial distance in an undisturbed magnetotail [*Arridge et al.*, 2009].

4. Discussion

[21] What is the global effect of solar wind compressions on Saturn's magnetospheric dynamics? Figure 4 is a schematic diagram that illustrates some features of the magnetospheric response that we have observed following a solar wind compression. With specific reference to the example shown here, we suggest that a solar wind compression impacted on Saturn's magnetosphere around the beginning of day 124 as evidenced by an increased solar wind dynamic pressure, and a strong SKR burst. This compression may have triggered a brief magnetotail reconnection event that resulted in plasmoid release and a TCR observation by Cassini that was positioned in the southern lobe. Such reconnection may in turn have played a role in further stimulating the SKR and triggering the low frequency radio emissions observed thereafter [e.g., *Louarn et al.*, 2007]. The magnetopause responded to the compression by briefly flaring and then became increasingly streamlined under the conditions of ongoing solar wind compression and high dynamic pressure. Over several subsequent days the field strength in the lobe was elevated. Slowly, the flaring angle started to increase, which we interpret as indicative of an increase in the amount of open flux contained in the tail. Such a sequence is commonly observed in the terrestrial magnetotail [*Milan et al.*, 2004]. We suggest that the tail flaring continuously varies to maintain stress balance between the elevated magnetic pressure in the magnetotail and the dynamic pressure in the magnetosheath.

[22] One of the main differences between Earth and Saturn is that the kronian tail lobes contain much more flux than the terrestrial ones, due to the much longer time scales required at Saturn to inflate the tail. *Badman et al.* [2005] noted that the flux content of Saturn's tail changes on a different timescale to the solar wind dynamic pressure changes and rather depends on the reconnection rate history as well as the solar wind conditions.

[23] Of course we do not have a monitor of the size of the polar cap at this time, but we can make a rough estimate of the amount of open flux that may have been added to the system through dayside reconnection during this period, based on the empirical formula put forward by *Jackman et al.* [2004] for the dayside reconnection voltage, Φ at Saturn:

$$\Phi = V_{SW} B_\perp L_0 \cos^4(\theta/2). \quad (2)$$

[24] We note that the average dayside reconnection rate obtained by *Jackman et al.* [2004] was ~50 kV, in good agreement with the in situ observations of dayside reconnection made by *McAndrews et al.* [2008]. Here we use the propagated model values for solar wind velocity, V_{sw}, $\boldsymbol{B}_\perp$, and clock angle θ, and take 10 R_S for the value of L_0, the

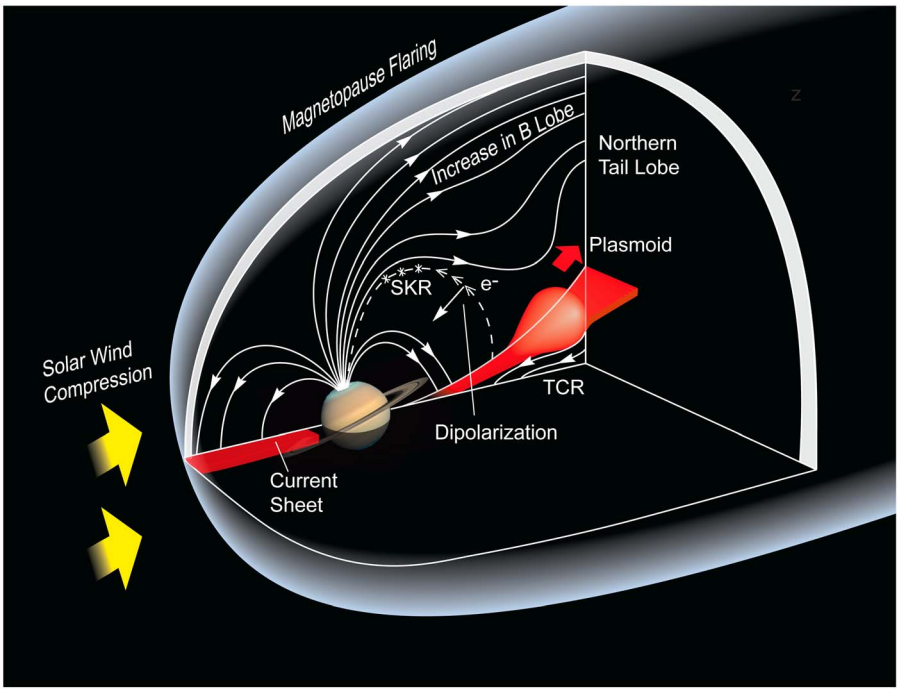

Figure 4. Schematic cartoon of some features of the magnetospheric response to a solar wind compression. These include changes in the degree of magnetopause flaring, increases in magnetotail lobe field strength under conditions of continued solar wind driving, magnetotail reconnection, precipitation of energetic electrons into the auroral zones, and stimulation of SKR emissions. The details of such responses, as manifested in the Cassini data, can be seen in Figures 2 and 3.

width of the solar wind channel in which the IMF reconnects with closed planetary field lines. From this we can estimate the expected dayside reconnection voltage, and thus, the cumulative open flux added to the magnetosphere. These quantities are shown in Figure 5. On the basis of the values plotted in Figure 5, we find that from the start of the interval to the start of day 131, we might expect that at least 20 GWb of open flux would have been added to Saturn's magnetosphere. Previous studies have led to estimates of the open flux content in each kronian tail lobe of ~35 GWb [*Ness et al.*, 1981; *Cowley and Bunce*, 2003; *Jackman et al.*, 2004]. By comparison with Earth, where tail reconnection closes ~40%–70% of the open flux contained in the tail at a given time [e.g., *Milan et al.*, 2003], at Saturn we might expect the flux content before tail reconnection to be of order ~45 GWb, and for each large reconnection event to close ~20–30 GWb. Thus, it does not seem inconceivable here for this 20 GWb of open flux addition between the start of the interval and the start of day 131 to be more than sufficient to trigger an episode of flux closure.

[25] However, a word of caution should be applied to this calculation: the solar wind propagation model IMF directions are not well constrained [*Zieger and Hansen*, 2008], and thus, there will be considerable error on the values of $\boldsymbol{B}_\perp$ and clock angle θ. For example, in this case, the propagated solar wind field directions yield a negative clock angle for ~7 days in a row. This is not a particularly accurate physical representation of the typical character of the solar wind upstream of Saturn, where the clock angle has been shown statistically to vary on time scales much shorter than 7 days [e.g., *Jackman et al.*, 2004, 2008b]. A clock angle that switches sign more frequently can make a big change to the expected rate of open flux production at the dayside magnetopause. For example, if we assume a steady $\boldsymbol{B}_\perp$ value of 0.5 nT and a clock angle of +45° (somewhat favorable for reconnection), we obtain a cumulative open flux value in excess of 60 GWb for the period ending day 131, in contrast to the 20 GWb estimate from the propagated values themselves. While equation (2) reflects a more gentle clock angle dependence, work by *Milan* [2004] incorporated the relation for dayside reconnection, whereby reconnection was ongoing for intervals of negative B_z (antiparallel IMF and terrestrial planetary field), and reconnection switched off entirely for intervals of positive B_z. We have incorporated this type of dependence (with opposite signs to reflect the direction of the kronian planetary field) with the red trace in Figure 5. Rather than use the propagated solar wind IMF directions, which we know to be poorly constrained, we have assumed a constant solar wind $\boldsymbol{B}_\perp$ of 0.5 nT and only used the propagated solar wind velocity values from the MSwiM model. We have assumed a pattern for the clock angle of alternating positive and negative values daily. The result is a reconnection voltage that varies daily from 0 V for negative clock angle (unfavorable for reconnection) to up to ~140 kV for positive clock angles. Under this regime, the cumulative open flux added to the system for the period ending day 131 is >40 GWb. On the basis of these additional calculations, we suggest that the 20 GWb derived directly from the *Jackman et al.* [2004] formula as applied directly to the MSwiM model outputs may represent quite a conservative estimate

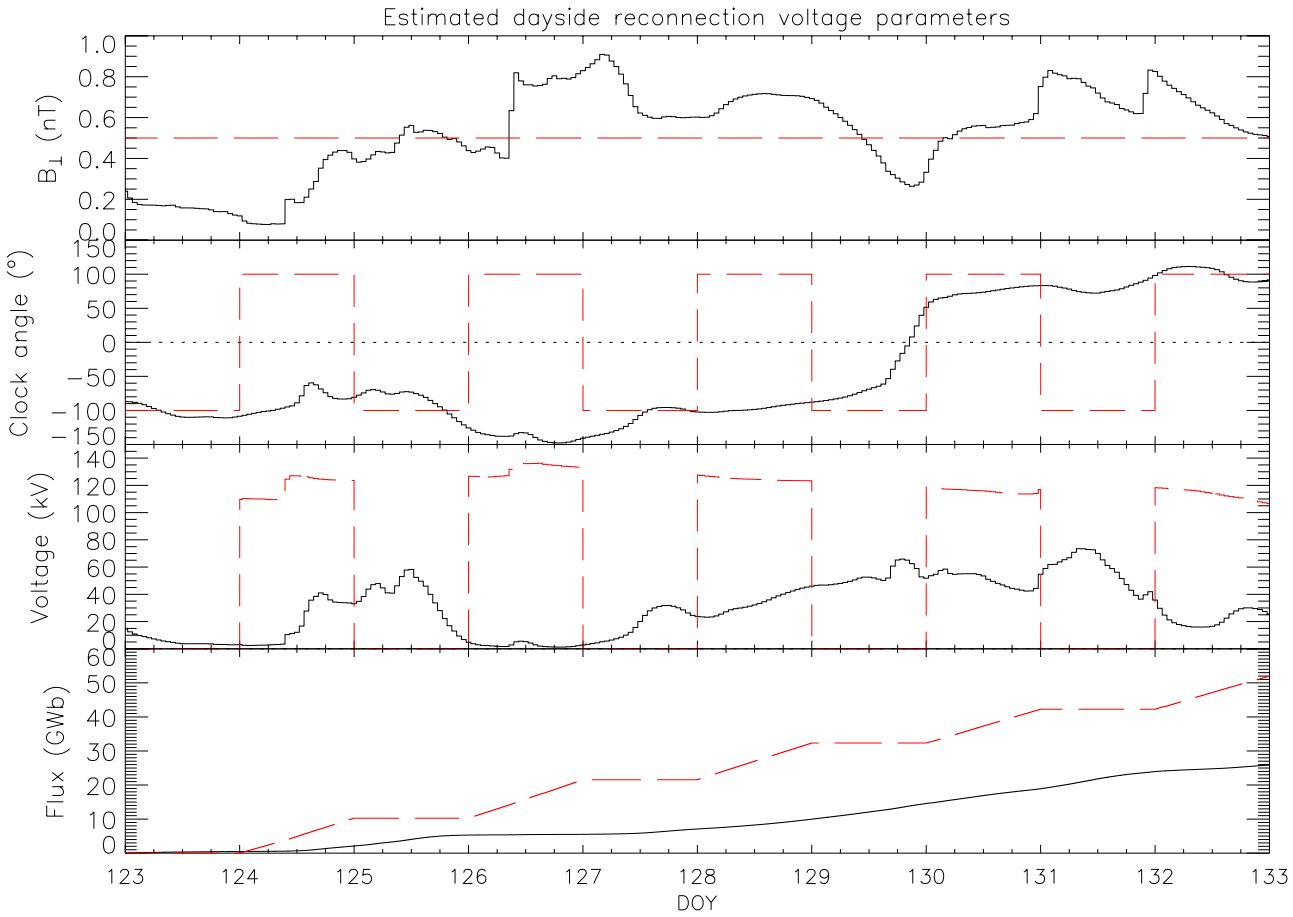

Figure 5. Plot of $\boldsymbol{B}_\perp$, clock angle θ, reconnection voltage Φ, and cumulative open flux as calculated from equation (2) for the interval 2006 days 123–133. $\boldsymbol{B}_\perp$ and θ are calculated based upon propagated solar wind parameters from the mSWiM model. The red dashed lines show an assumed constant value for $\boldsymbol{B}_\perp$, a daily varying clock angle θ, and the resultant reconnection voltage and cumulative flux values based on the reconnection voltage formula outlined by *Milan* [2004].

of the amount of open flux added to the system during this interval. Indeed, after observing elevated field strengths for ~7 days, we suggest that the magnetotail lobes easily contained sufficient stored magnetic flux for a critical threshold to be exceeded and reconnection to be stimulated. On day 131 we see a northward turning of the field that we suggest is the signature of a passing plasmoid, released during a magnetotail reconnection event stimulated by the need for the magnetosphere to expel some of the flux accumulated during the previous days.

[26] Another feature to note is that, despite maintaining an approximately constant latitude, the spacecraft went from observing the southern lobe almost continuously from day 125 onward, to encountering the current sheet at the start of day 131. We suggest that this encounter may be the signature of a deflection or "flop" of the current sheet from its hinged position down toward the equator. *Arridge et al.* [2008] noted that the hinging distance will be a function of the solar wind dynamic pressure, which was slowly falling toward the end of the interval shown in Figure 1. *Khurana et al.* [2009] commented that at large radial distances from the planet, the current sheet shape and location is determined by the magnetopause shape. Thus, any deflation of the magnetosphere as a whole (which seems plausible within the error of our flaring estimates) may be related to the motion of the current sheet down toward the equator.

[27] Our aim in this paper was to draw together the sequence of events that can typically occur when a solar wind compression impacts on Saturn's magnetosphere. In this example, we see strong evidence for a solar wind compression, manifested by jumps in solar wind velocity and dynamic pressure, and intense SKR emission. The magnetosphere initially became more streamlined, and the lobe field strength became elevated as external pressure compressed the tail. Then assuming a favorable IMF direction (for at least part of the interval, as seems entirely plausible), dayside reconnection may have been ongoing, leading to an increase in the amount of open flux inside the magnetosphere, flaring of the magnetotail, and continued elevated lobe field strength. Because of the longer time scales involved at Saturn for loading of the tail with open flux, it can take several days for the tail to be inflated to a point where reconnection is likely to occur, and we suggest that the time scale observed in this case was of order ~6–7 days. We see no strong evidence for magnetotail

reconnection events during this loading phase. However, toward the end of this we observe a sharp decrease in lobe field strength and what appears to be significant current sheet deflection toward the equator from its previously hinged position. We suggest that the subsequent northward turnings of the field are evidence of magnetic reconnection in the tail in the form of plasmoid and TCR signatures. These field signatures are closely correlated with intense radio emission, evidenced by low-frequency extensions of radio emission. Finally, the magnetotail returned to "quiet" conditions. The frequency, strength, and global influence of magnetotail reconnection events at Saturn is a topic of considerable interest currently, and further work will explore the relative roles of external triggering and internal flux thresholds for such processes.

[28] **Acknowledgments.** Cassini data activities at Imperial College and Mullard Space Science Laboratory were funded by Science and Technology Facilities Council. C.M.J. would like to thank Neal Powell at Imperial for artwork. C.S.A. was funded by an STFC Postdoctoral fellowship under grant ST/G007462/1. C.S.A. would like to thank G.-R. Fouad for useful discussions. We thank K.C. Hansen and B. Zieger for providing solar wind propagations from their Michigan Solar Wind Model. We acknowledge P. Zarka and B. Cecconi for development of RPWS data processing and the support of the CNES agency.

[29] Masaki Fujimoto thanks the reviewers for their assistance in evaluating this article.

References

Achilleos, N., et al. (2006), Orientation, location, and velocity of Saturn's bow shock: Initial results from the Cassini spacecraft, *J. Geophys. Res.*, *111*, A03201, doi:10.1029/2005JA011297.

Arridge, C. S., N. Achilleos, M. K. Dougherty, K. K. Khurana, and C. T. Russell (2006), Modeling the size and shape of Saturn's magnetopause with variable dynamic pressure, *J. Geophys. Res.*, *111*, A11227, doi:10.1029/2005JA011574.

Arridge, C. S., et al. (2009), Plasma electrons in Saturn's magnetotail: Structure, distribution, and energization, *Planet. Space. Sci.*, *57*, 2032–2047, doi:10.1016/j.pss.2009.09.007.

Arridge, C. S., K. K. Khurana, C. T. Russell, D. J. Southwood, N. Achilleos, M. K. Dougherty, A. J. Coates, and H. K. Leinweber (2008), Warping of Saturn's magnetospheric and magnetotail current sheets, *J. Geophys. Res.*, *113*, A08217, doi:10.1029/2007JA012963.

Badman, S. V., E. J. Bunce, J. T. Clarke, S. W. H. Cowley, J.-C. Gérard, D. Grodent, and S. E. Milan (2005), Open flux estimates in Saturn's magnetosphere during the January 2004 Cassini-HST campaign and implications for reconnection rates, *J. Geophys. Res.*, *110*, A11216, doi:10.1029/2005JA011240.

Boudouridis, A., E. Zesta, L. R. Lyons, P. C. Anderson, and D. Lummerzheim (2003), Effect of solar wind pressure pulses on the size and strength of the auroral oval, *J. Geophys. Res.*, *108*(A4), 8012, doi:10.1029/2002JA009373.

Bunce, E. J., S. W. H. Cowley, D. M. Wright, A. J. Coates, M. K. Dougherty, N. Krupp, W. S. Kurth, and A. M. Rymer (2005), In situ observations of a solar wind compression-induced hot plasma injection in Saturn's tail, *Geophys. Res. Lett.*, *32*, L20S04, doi:10.1029/2005GL022888.

Clarke, J. T., et al. (2005), Morphological differences between Saturn's ultraviolet aurorae and those of Earth and Jupiter, *Nature*, *433*, 717–719.

Collier, M. R., J. A. Slavin, R. P. Lepping, K. Ogilvie, A. Szabo, H. Laakso, and S. Taguchi (1998), Multispacecraft observations of sudden impulses in the magnetotail caused by solar wind pressure discontinuities: Wind and IMP 8, *J. Geophys. Res.*, *103*, 17293, doi:10.1029/97JA02870.

Coroniti, F. V., and C. F. Kennel (1972), Changes in magnetospheric configuration during the substorm growth phase, *J. Geophys. Res.*, *77*, 3361, doi:10.1029/JA077i019p03361.

Cowley, S. W. H., and E. J. Bunce (2003), Corotation-driven magnetosphere-ionosphere coupling currents in Saturn's magnetosphere and their relation to the auroras, *Ann. Geophys.*, *21*(8), 1691–1707.

Cowley, S. W. H., S. V. Badman, E. J. Bunce, J. T. Clarke, J.-C. Gérard, D. Grodent, C. M. Jackman, S. E. Milan, and T. K. Yeoman (2005), Reconnection in a rotation-dominated magnetosphere and its relation to Saturn's auroral dynamics, *J. Geophys. Res.*, *110*, A02201, doi:10.1029/2004JA010796.

Crary, F. J., et al. (2005), Solar wind dynamic pressure and electric field as the main factors controlling Saturn's auroras, *Nature*, *433*, 720–722.

Desch, M. D., and H. O. Rucker (1983), The relationship between Saturn kilometric radiation and the solar wind, *J. Geophys. Res.*, *88*, 8999–9006, doi:10.1029/JA088iA11p08999.

Dougherty, M. K., et al. (2004), The Cassini magnetic field investigation, *Space Sci. Rev.*, *114*, 331–383.

Gurnett, D. A. (1974), The Earth as a radio source: Terrestrial kilometric radiation, *J. Geophys. Res.*, *79*, 4227–4238, doi:10.1029/JA079i028p04227.

Gurnett, D. A., W. S. Kurth, and F. L. Scarf (1981), Narrowband electromagnetic radiation from Saturn's magnetosphere, *Nature*, *292*, 733–737, doi:10.1038/292733a0.

Gurnett, D. A., et al. (2004), The Cassini radio and plasma wave investigation, *Space Sci. Rev.*, *114*, 395–463.

Hill, T. W., et al. (2008), Plasmoids in Saturn's magnetotail, *J. Geophys. Res.*, *113*, A01214, doi:10.1029/2007JA012626.

Hubert, B., M. Palmroth, T. V. Laitinen, P. Janhunen, S. E. Milan, A. Grocott, S. W. H. Cowley, T. Pulkkinen, and J.-C. Gérard (2006), Compression of the Earth's magnetotail by interplanetary shocks directly drives transient magnetic flux closure, *Geophys. Res. Lett.*, *33*, L10105, doi:10.1029/2006GL026008.

Huttunen, K. E. J., J. Slavin, M. Collier, H. E. J. Koskinen, A. Szabo, E. Tanskanen, A. Balogh, E. Lucek, and H. Rème (2005), Cluster observations of sudden impulses in the magnetotail caused by interplanetary shocks and pressure increases, *Ann. Geophys.*, *23*, 609–624.

Isbell, J., A. J. Dessler, and J. H. Hunter Jr. (1984), Magnetospheric energization by interaction between planetary spin and the solar wind, *J. Geophys. Res.*, *89*, 10,716–10,722, doi:10.1029/JA089iA12p10716.

Jackman, C. M., N. Achilleos, E. J. Bunce, S. W. H. Cowley, M. K. Dougherty, G. H. Jones, S. E. Milan, and E. J. Smith (2004), Interplanetary magnetic field at ~9 AU during the declining phase of the solar cycle and its implications for Saturn's magnetospheric dynamics, *J. Geophys. Res.*, *109*, A11203, doi:10.1029/2004JA010614.

Jackman, C. M., N. Achilleos, E. J. Bunce, B. Cecconi, J. T. Clarke, S. W. H. Cowley, W. S. Kurth, and P. Zarka (2005), Interplanetary conditions and magnetospheric dynamics during the Cassini orbit insertion fly-through of Saturn's magnetosphere, *J. Geophys. Res.*, *110*, A10212, doi:10.1029/2005JA011054.

Jackman, C. M., C. T. Russell, D. J. Southwood, C. S. Arridge, N. Achilleos, and M. K. Dougherty (2007), Strong field dipolarizations in Saturn's magnetotail: In situ evidence of reconnection, *Geophys. Res. Lett.*, *34*, L11203, doi:10.1029/2007GL029764.

Jackman, C. M., et al. (2008a), A multi-instrument view of tail reconnection at Saturn, *J. Geophys. Res.*, *113*, A11213, doi:10.1029/2008JA013592.

Jackman, C. M., R. J. Forsyth, and M. K. Dougherty (2008b), The overall configuration of the interplanetary magnetic field upstream of Saturn as revealed by Cassini observations, *J. Geophys. Res.*, *113*, A08114, doi:10.1029/2008JA013083.

Jackman, C. M., L. Lamy, M. P. Freeman, P. Zarka, B. Cecconi, W. S. Kurth, S. W.H. Cowley, and M. K. Dougherty (2009a), On the character and distribution of lower-frequency radio emissions at Saturn and their relationship to substorm-like events, *J. Geophys. Res.*, *114*, A08211, doi:10.1029/2008JA013997.

Jackman, C. M., et al. (2009b), Properties of the magnetic field and plasma in the kronian magnetotail lobes and current sheet, presented at the American Geophysical Union Fall Meeting, San Francisco, Calif.

Jackman, C. M., C. S. Arridge, H. J. McAndrews, M. G. Henderson, and R. J. Wilson (2009c), Northward field excursions in Saturn's magnetotail and their relationship to magnetospheric periodicities, *Geophys. Res. Lett.*, *36*, L16101, doi:10.1029/2009GL039149.

Khurana, K. K., D. G. Mitchell, C. S. Arridge, M. K. Dougherty, C. T. Russell, C. Paranicas, N. Krupp, and A. J. Coates (2009), Sources of rotational signals in Saturn's magnetosphere, *J. Geophys. Res.*, *114*, A02211, doi:10.1029/2008JA013312.

Kurth, W. S., et al. (2005), An Earth-like correspondence between Saturn's auroral features and radio emission, *Nature*, *433*, 722–725, doi:10.1038/nature03334.

Lamy, L., P. Zarka, B. Cecconi, R. Prange, W. S. Kurth, and D. A. Gurnett (2008), Saturn kilometric radiation: Average and statistical properties, *J. Geophys. Res.*, *113*, A07201, doi:10.1029/2007JA012900.

Louarn, P., et al. (2007), Observation of similar radio signatures at Saturn and Jupiter: Implications for the magnetospheric dynamics, *Geophys. Res. Lett.*, *34*, L20113, doi:10.1029/2007GL030368.

McAndrews, H. J., C. J. Owen, M. Thomsen, B. Lavraud, A. Coates, M. Dougherty, and D. T. Young (2008), Evidence for reconnection at Saturn's magnetopause, *J. Geophys. Res.*, *113*, A04210, doi:10.1029/2007JA012581.

McPherron, R. (1970), Growth phase of magnetospheric substorms, *J. Geophys. Res.*, *75*, 5592–5599, doi:10.1029/JA075i028p05592.
Milan, S. E., M. Lester, S. W. H. Cowley, K. Oksavik, M. Brittnacher, R. A. Greenwald, G. Sofko, and J.-P. Villain (2003), Variations in polar cap area during two substorm cycles, *Ann. Geophys.*, *21*(5), 1121–1140.
Milan, S. E. (2004), A simple model of the flux content of the distant magnetotail, *J. Geophys. Res.*, *109*, A07210, doi:10.1029/2004JA010397.
Milan, S. E., S. W. H. Cowley, M. Lester, D. M. Wright, J. A. Slavin, M. Fillingim, C. W. Carlson, and H. J. Singer (2004), Response of the magnetotail to changes in the open flux content of the magnetosphere, *J. Geophys. Res.*, *109*, A04220, doi:10.1029/2003JA010350.
Milan, S. E., E. J. Bunce, S. W. H. Cowley, and C. M. Jackman (2005), Implications of rapid planetary rotation for the Dungey magnetotail of Saturn, *J. Geophys. Res.*, *110*, A03209, doi:10.1029/2004JA010716.
Milan, S. E., G. Provan, and B. Hubert (2007), Magnetic flux transport in the Dungey cycle: A survey of dayside and nightside reconnection rates, *J. Geophys. Res.*, *112*, A01209, doi:10.1029/2006JA011642.
Milan, S. E., P. D. Boakes, and B. Hubert (2008), Response of the expanding/contracting polar cap to weak and strong solar wind driving: Implications for substorm onset, *J. Geophys. Res.*, *113*, A09215, doi:10.1029/2008JA013340.
Morioka, A., et al. (2008), AKR breakup and auroral particle acceleration, *J. Geophys. Res.*, *113*, A09213, doi:10.1029/2008JA013322.
Ness, N. F., M. H. Acuña, R. P. Lepping, J. E. P. Connerney, K. W. Behannon, L. F. Burlaga, and F. M. Neubauer (1981), Magnetic field studies by Voyager 1: Preliminary results at Saturn, *Science*, *212*, 211–217.
Petrinec, S. M., and C. T. Russell (1996), Near-Earth magnetotail shape and size as determined from the magnetopause flaring angle, *J. Geophys. Res.*, *101*, 137–152, doi:10.1029/95JA02834.
Russell, C. T., and R. L. McPherron (1973), The magnetotail and substorms, *Space Sci. Rev.*, *15*, 205–266.
Slavin, J., E. Smith, B. Tsurutani, D. Sibeck, H. Singer, D. Baker, J. Gosling, E. Hones, and F. Scarf (1984), Substorm-associated traveling compression regions in the distant tail: Isee-3 geotail observations, *Geophys. Res. Lett.*, *11*, 657–660, doi:10.1029/GL011i007p00657.
Slavin, J. A., E. J. Smith, D. G. Sibeck, D. N. Baker, R. D. Zwickl, and S. I. Akasofu (1985), An ISEE 3 study of average and substorm conditions in the distant magnetotail, *J. Geophys. Res.*, *90*, 10,875–10,895, doi:10.1029/JA090iA11p10875.
Ye, S.-Y., D. A. Gurnett, G. Fischer, B. Cecconi, J. D. Menietti, W. S. Kurth, Z. Wang, G. B. Hospodarsky, P. Zarka, and A. Lecacheux (2009), Source locations of narrowband radio emissions detected at Saturn, *J. Geophys. Res.*, *114*, A06219, doi:10.1029/2008JA013855.
Young, D. T., et al. (2004), Cassini plasma spectrometer investigation, *Space Sci. Rev.*, *114*, 1–112.
Zieger, B., and K. C. Hansen (2008), Statistical validation of a solar wind propagation model from 1 to 10 AU, *J. Geophys. Res.*, *113*, A08107, doi:10.1029/2008JA013046.

C. S. Arridge and A. J. Coates, Mullard Space Science Laboratory, Department of Space and Climate Physics, University College London, Dorking RH5 6NT, UK.
M. K. Dougherty, C. M. Jackman, and L. Lamy, Blackett Laboratory, Imperial College London, Prince Consort Road, London SW7 2BW, UK. (c.jackman@imperial.ac.uk)
S. E. Milan, Radio and Space Plasma Physics Group, University of Leicester, University Rd., Leicester LE1 7RH, UK.
J. A. Slavin, Heliophysics Science Division, NASA Goddard Space Flight Center, Greenbelt, MD 20771, USA.